Title
PARTICLE IRRADIATION METHODS. CHAPTER 3

Authors
Raju, M.R.
Lyman, J.T.
Tobias, C.A.

Publication Date
1971-03-01

To be published as a
Chapter in book "Space Radiology",
C. A. Tobias and P. W. Todd, Editors
(Academic Press, NY)

UCRL-20226
Preprint

CHAPTER 3. PARTICLE IRRADIATION METHODS

M. R. Raju, J. T. Lyman, and C. A. Tobias

March 1971

AEC Contract No. W-7405-eng-48

LAWRENCE RADIATION LABORATORY
UNIVERSITY of CALIFORNIA BERKELEY

DISCLAIMER

CHAPTER 3. PARTICLE IRRADIATION METHODS

M. R. Raju, J. T. Lyman and C. A. Tobias

Donner Laboratory and Donner Pavilion
Lawrence Radiation Laboratory
University of California
Berkeley, California
94720

1. Introduction

Astonishing progress has been achieved in the study of various components of cosmic and solar radiation by means of Earth-based methods, balloon flights, rocket flights, and many detailed experiments in satellites, so that we have a good idea of the atomic number, flux, energy distribution, and time distribution of the various types of events (see Chapter 2).

For the safety of astronauts, it is necessary to have detailed knowledge of the effects of solar particles and of cosmic radiations. The need to develop a biological oxygen-generating system with the use of plants or populations of plant cells implies that we must also understand the behavior of such systems under continuous and intermittent radiation. In order to answer basic problems of space biology with regard to the role of radiation in the origin of organic molecules and perhaps of life, for understanding what limits radiation may place on life at the surface of planets, and for testing the theoretical ideas for transmigration of life in space, it is necessary to have a detailed understanding of the radiobiology of fast heavy charged particles on a number of test objects: molecules, cells, plants, animals, and man.

Although biological organisms have been flown in a number of satellites, we cannot at present expect a detailed solution for all space radiobiological problems from satellite flights. The background dose is usually quite low. Solar flares cannot be predicted far enough in advance to orbit biological specimens in that part of space that may be exposed in a given flare. The understanding of the effects of long-term low-intensity radiation would necessitate many long-term space flights. Even if all these experiments were feasible in space, one would need large numbers of individuals exposed to obtain statistically significant information. The costs of such efforts would be staggering and the

manpower needed for performing such studies impractically large.

A logical way of proceeding in space radiobiological studies is to study the effects of particles in accelerators at ground level. Electrons, protons, and helium ions--some of the major solar particles--have been accelerated in a number of machines to all pertinent energies that occur in solar flares and in the radiation belt. Some of the heavier ions have also been accelerated to relatively low energies sufficient to study some molecular and cellular effects. For the future, several methods of acceleration are under development. These will allow scientists to accelerate virtually all stable nuclei in the periodic table to energies of several hundred MeV per nucleon at sufficiently high fluxes to make rapid progress in heavy-ion radiobiology possible.

Even with fairly thorough studies with accelerators, additional space experiments may be necessary to verify the findings obtained at ground level. Since experimental exposure of man is not feasible, most of our knowledge of effects on humans comes from extrapolation of animal data or from radiological experience with patients. Pertinent studies on astronauts in space flight may help to verify the validity of such extrapolations.

It is necessary to study possible synergisms or antagonisms between radiation effects and space environment. Weightlessness is the most important such factor. Although it is possible to "compensate" gravitational forces in clinostats, this type of "compensation" is not the same as weightlessness in space. Some biological experiments in the near-weightless condition in satellites have already been performed (see Chapter 7). It is nevertheless considerably less expensive to seek preliminary answers to pertinent problems of space radiation and weightlessness by use of clinostats and accelerators.

1.1. Biological Use of Accelerators

Biological studies with accelerated particles began in 1947 (Tobias et al., 1952), one year before atomic nuclei in primary cosmic rays were discovered and 10 years before the first manned space flight (Chapter 1). Most of these studies utilized machines that were built for the primary purpose of physics research; the parameters were not always optimal for biological uses.

The typical medium-energy cyclotrons used for biological research have near-monoenergetic and parallel beams. At present in most of these machines it is not feasible to vary the energy. For intermediate energies, absorbers and scatterers are used to degrade the beams. This is sometimes not desirable, since secondary

particles are produced that contaminate the primary beams, and the particles increase their angular divergence. Nevertheless, it was possible to produce at the Berkeley synchrocyclotron beams with the desired energy distribution that simulate a solar flare spectrum. The simulation is fairly good in both spatial dose distribution and LET distribution. The simulation is not perfect, however, since cyclotron particles come in pulses of a few microseconds each, not continuously like flares. In addition, many other techniques are available that will deliver a beam of precisely controlled LET to a predetermined location and depth in the body. In some space-related problems, this is important. For example, in studying the effects of radiation on the vestibular system-- an important problem in space flight--it is an advantage to determine, by local radiation methods, whether the proprioceptors, the semicircular canal, or perhaps the vestibular nuclei of the brain are responsible for radiation-induced alteration in the sense of equilibrium.

Table 3.1 presents a list of a few accelerators that have been used in biological studies related to space. We have made no attempt to include all accelerators that could be useful in this regard. Accelerator lists have been compiled (Gordon and Behman, 1963).

Two chapters in this book deal directly with the measured biological effects of particulate radiations: Chapter 5, "Cellular Radiation Biology," and Chapter 9, "Particulate Irradiation of Mammals." The performance of the experiments depended upon a reliable source of high-speed charged particles and accurate means to measure their energies, LET's, dose distributions, etc. We therefore deal briefly in this chapter with the properties of high-speed charged particles, techniques of dose measurement, profiles of charged-particle beams, techniques and equipment specifically designed for the exposure of biological test objects, methods of producing programmed depth-dose patterns and programmed energy spectra at high energies, and the probable directions of future undertakings.

2. Heavy-Charged-Particle Properties

Heavy charged particles in passing through matter lose energy chiefly through interactions with atomic electrons. This process leads to a gradual decrease of energy until the particles are slowed down to the thermal energy of the matter. The rate of energy loss increases with decreasing particle velocity, giving rise to a sharp maximum known as the Bragg peak near the end of the particle range. The rate of energy loss is proportional to the square of the charge on the particle and approximately inversely proportional to the square of the particle velocity. When the particle velocity is

very low the particles capture electrons and hence their effective charge is reduced, resulting in a decrease of the rate of energy loss (see Northcliffe, 1963). The average rate of energy loss is commonly expressed in MeV per g/cm^2. This is sometimes referred to as mass stopping power.

The particles in the beam that do not undergo nuclear interactions travel approximately equal path lengths in the medium. The particle interactions with electrons in the medium are subject to statistical fluctuations, and hence there are fluctuations in the path lengths of the individual particles. This is called range straggling, and it is about 1% of the mean path length, or range (Wilson, 1946). Since the particles encountered in the space environment are inhomogeneous in energy, range straggling is not an important consideration in flares. However, it is important for laboratory studies. Range and stopping power in water for different heavy ions are shown in Fig. 3.1. Tables of range and mass stopping power are available (Barkas and Berger, 1964; Williamson et al., 1966; Janni, 1966; Trower, 1966; Bichsel, 1968).

As charged particles pass through matter, some are removed from the beam due to nuclear interactions. This particle loss is exponential, at a rate depending upon the total reaction cross section σ_R. An approximate expression for σ_R is given by

$$\sigma_R \approx \pi r_0^2 ([A_T]^{1/3} + [A_I]^{1/3}), \qquad (3-1)$$

where r_o is the classical proton radius, A is the atomic weight, and subscripts T and I refer to the target and the incident particles, respectively (see Rossi, 1952).

The number of particles surviving at a given depth in any medium can be estimated from the mean free path L for the particles in that medium. The expression for the mean free path L in g/cm^2 is given by

$$L = A_T/(\sigma_R N_0), \qquad (3-2)$$

where N_o is Avogadro's number.

When a parallel beam of heavy charged particles passes through a medium, the particles are scattered and the beam diameter increases with depth, mainly due to Coulomb-force interactions

between the incident particle and nuclei of the medium. This scattering is due partly to the cumulative effect of many small deflections, and partly to large single-event deflections of relatively few of the particles. The first type of process is called multiple scattering; the second is referred to as single scattering. For most practical applications multiple scattering,which can be represented approximately by a Gaussian distribution, predominates over single scattering.
The mass of a heavy charged particle is many times that of the electron; the angle of scattering in a given collision is reduced approximately by the ratio of masses. Hence heavy charged particles produce a more sharply defined beam than electrons of comparable velocity.

Preston and Koehler (1968) obtained an empirical expression for the radial standard deviation σ_0 in centimeters at the end of the range R_0 (cm) due to multiple scattering for a proton beam of originally negligible diameter,

$$\sigma_o=0.0307R_o. \qquad (3-3)$$

For beams of radii much greater than σ_o, the effects of multiple scattering on the radial spread of the beam are negligible except at the periphery of the beam. The scattering "rounds off " the profiles that were initially, say, rectangular. For small beams of radii $<3\sigma_o$, the central axis depth dose at the peak will be significantly reduced below that from broader beams.

3. Detectors

Many types of detectors are used in heavy-charged-particle irradiation techniques for experimental space radiobiology. The principles of operation and the design of these detectors are not discussed except to mention some of the important aspects of the detectors most commonly used (see Raju et al., 1969). A detailed discussion of various radiation dosimeters can be found in Radiation Dosimetry, 2nd Ed. (Attix, Roesch, and Tochilin, 1966).

3.1. Ionization Chambers

A parallel-plate ionization chamber is the most commonly used detector to monitor charged-particle beam intensity and to measure radiation dose. The relationship between the charge Q

(coulombs) collected in the ionization chamber and the dose D (rads) absorbed in the sensitive volume of the ionization chamber is given by

$$D = 10^5 QW/(\rho V), \qquad (3-4)$$

where W is the average energy per ion pair (eV) for the chamber gas, ρ is the density (g/cm^2) of the gas, and V (cm^3) is the sensitive volume of the ionization chamber. The dose received by the target material, such as tissue, can be calculated by multiplying this dose value by the ratio of mass stopping power of the target material to that of the gas.

3.2. Faraday Cup

The Faraday cup (Chamberlain et al., 1951; Palmieri and Goloskie, 1964; Santoro and Peele, 1964) is often used as a primary standard to determine the number of particles in a charged-particle beam. The charge-collection efficiency of a well-designed cup is independent of the beam intensity. The Faraday cup consists of an absorber block, thick enough to stop all the primary beam and its secondary charged particles. This block, generally cup-shaped, is supported by insulators within an evacuated chamber. Care must be taken in designing the Faraday cup so that the net charge collected is only that delivered by the beam (Raju et al., 1969).

The number of particles N stopped in a Faraday cup is given by the relation

$$N = Q_F/(ze), \qquad (3-5)$$

where Q_F is the charge (in coulombs) collected, z is the average number of charges carried per particle, and e is the electronic charge in coulombs. Knowing the particle fluence Φ (particles/cm^2) in the target material, one can calculate the dose D, in rads, from

$$D = 1.602\Phi\,(-1/\rho x dT/dx) \times 10^{-8}, \qquad (3-6)$$

where $(-1/\rho x dT/dx)$ is the mass stopping power of the target material in MeV-em^2/g.

3.3. Secondary-Emission Monitor

The secondary-emission monitor (SEM) is particularly useful in high-intensity radiation fields where ionization chambers cannot be used because of incomplete ion collection due to recombination (Tautfest and Fechter, 1955). In a SEM the charge is due to the transfer of low-energy secondary electrons between the high-voltage electrode and the collection electrode, in ultrahigh vacuum ($\approx 10^{-8}$ torr). It is calibrated by using an ionization chamber at a low beam intensity.

3.4. Activation Dosimeter

Heavy charged particles produce radioactive isotopes as a result of inelastic nuclear reactions. The induced activity of the sample may be used to determine either the particle flux (particles/sec) in the entire beam, or the particle flux density (particles/cm^2-sec) within a small area of the beam, depending on the geometric arrangement of the irradiation. Activation by charged-particle beams has been extensively treated by Tilbury (1966). The general techniques and computational approach are similar to those encountered in neutron-activation dosimetry.

One of the most commonly used reactions for activation dosimetry of high-energy protons is $^{12}C(p,pn)^{11}C$. The gamma radiation from the annihilation of the positron from the decay of ^{11}C (half-life 20.5 min) is usually counted with a pair of scintillation detectors. Polyethylene (CH_2) is usually employed as the carbon-bearing material (Jesseph et al., 1968). The induced activity in tissue can also be utilized (Benson et al., 1967). Other useful radioisotopes produced in charged-particle irradiated tissue are the positron emitters ^{13}N (half-life 9.96 min) and ^{15}O (2.1 min).

3.5. Semiconductor Detector

Semiconductor detectors are solid-state analogs of ionization chambers, the charge carriers being electrons and holes. The use of a solid as a detector is attractive because the sensitive layer can be very thin while still absorbing enough energy to give good

sensitivity. The sensitivity is further enhanced because of the small amount of energy required to produce an electron–hole pair (≈3.75 eV in silicon) (Goulding, 1965). This leads to smaller statistical fluctuations in the number of electron–hole pairs and, hence, improved energy resolution over that of gas-filled and scintillation counters having comparable energy absorption. An attractive feature of these detectors is that their response is proportional to the deposited energy, independent of the particle (Lyman, 1965). These detectors are used in measuring energy and energy losses of heavy charged particles in a spatially defined, region (Maccabee et al., 1968; Raju, 1967).

4. Beam Measurements

The radiation field of an accelerator beam is characterized by measurements such as Bragg ionization curve, integral range curve,energy loss distribution, isodose contours, etc. These measurements are briefly discussed below.

4.1. The Bragg Ionization Curve

A Bragg curve is a plot of the relative specific ionization of a collimated beam of particles, plotted as a function of the thickness of absorber that the beam has traversed (Bragg, 1904). It can be obtained experimentally by taking the ratio of current from two ionization chambers, as shown in Fig. 3.2. A monitor chamber is placed ahead of a variable absorber, and a second chamber is placed behind the absorber. The shape of a Bragg curve is dependent upon many factors, mainly the energy and the energy spread of the initial beam, the nature of the incident particle, and the nature of the absorbing material. Since the amount of straggling increases almost linearly with the thickness of absorber, monoenergetic parallel beams of low energy show the sharpest Bragg peaks.

In Bragg–curve measurements, secondary particles from collimators used to define the beam should not contribute to the ionization in the second ionization chamber. In addition, the second ionization chamber, which detects the transmitted beam from the variable absorber, should have a collecting electrode with diameter large enough to cover the entire area of the transmitted beam. If the collecting electrode is much smaller than the beam diameter a different experimental curve known as the central–axis depth–dose distribution is obtained. Such curves for beams of protons and helium ions of several energies are shown in Fig. 3.3.

The dose delivered to the medium at the beam entrance is called the "plateau dose," and the dose at the Bragg peak the "peak dose."

The peak-to-plateau ratio is a very sensitive function of momentum spread (the same effect as energy spread) of the beam. With increasing momentum spread, the peak-to-plateau ratio is reduced considerably, with concomitant increase in the width of the Bragg peak. With increasing energy and hence increasing range of the particles, the range straggling increases. This effect reduces the peak-to-plateau ratio and broadens the peak of the curve. In addition, with increasing energy of the particles more particles are removed from the beam because of nuclear interactions before they reach the Bragg peak, and this also results in a reduction in peak-to-plateau ratio. A computer program for calculating Bragg curves for heavy-ion beams is available (Litton et al.,1968).

4.2. Integral Range Curves

A plot of the number of particles that have passed through an absorber as a function of absorber thickness is called an integral range curve or a number-distance curve. The number of charged particles that have passed through an absorber can be determined with particle counters or a Faraday cup. The experimental arrangement used to determine an integral range curve is similar to that shown in Fig. 3.2, but with the second ionization chamber replaced by a particle counter or a Faraday cup. For low-energy particles for which nuclear interactions can be neglected, the number of particles remains essentially constant from zero absorber to a thickness slightly less than the mean range of the particles. At high energies, particles are lost from the beam by nuclear interactions. Then the integral range curve as shown in Fig. 3.4 for a 910-MeV helium-ion beam has a negative slope. An estimate of the cross section for the nuclear interactions can be obtained from this slope. The contribution to the Faraday cup current beyond the range of the helium ion beam is due to nuclear secondaries produced by the primary beam in the absorbing material.

An estimate of the range of the particles can be obtained by considering the tail of the integral range curve (Santoro, 1965; Santoro et al., 1966). A useful reference point is the extrapolated range, which can be obtained by drawing the tangent to the integral range curve at the point of steepest slope and extrapolating it to the horizontal axis.

4.3. Beam Profile and Isodose Contours

For many applications of heavy-charged-particle beams, one needs to know the three-dimensional dose distribution in the irradiated material. For such measurements, the sensitive area of

the detector should be kept small relative to the cross section of the beam. At the same time the detector must have adequate sensitivity. Small semiconductor devices are suitable for this application. An example of such a semiconductor device is a miniature silicon diode 0.1 cm in maximum diameter and 0.22 cm long (Koehler, 1967; Raju, 1966).

Profiles can also be measured by using such equipment as ionization chambers, particle counters, photographic film, activation analysis, or thermoluminescent dosimeters. From a series of beam profiles, a set of isodose contours can be constructed. Figure 3.5 shows such an isodose plot for a degraded 910-MeV helium-ion beam in water.

If the profile itself is changing with time, continous display of the profile is necessary (Jackson et al., 1959; Bewley et al., 1967; Hornstra and Simanton, 1969).

A continuous monitor to reflect such changes is quite useful. A beam position monitor routinely used at the Berkeley heavy-ion linear accelerator displays a pattern representing the beam on an x-y oscilloscope. The pattern is circular when the beam is circular and elliptical when the beam is elliptical. Four detectors are used to detect the beam, one pair oriented horizontally and the other vertically. The detectors could be a quadrant ionization chamber, or sectored collimator used as a Faraday cup. A difference signal developed from the vertical detectors positions the oscilloscope pattern in the vertical plane, while a difference signal from the horizontal detectors positions the pattern in the horizontal plane. A sum signal from each detector pair modulates the amplitude of quadrature sine waves which generate the pattern.

5. Irradiation Techniques

Electrons, protons, and heavier particles with a broad spectrum of energies are encountered in space. In order to predict the biological effects of such a complex radiation environment, one has to study the effects of individual components. Proton and heavy-particle irradiation techniques at heavy-particle accelerators are discussed. The techniques of exposure can be broadly classified depending on the thickness of the biological sample in comparison with the range of the particle used:

(a) Samples much smaller than the range of the particle.
(b) Samples much larger than the range of the particle.
(c) Intermediate cases.

5.1. Samples Much Smaller Than the Range of the Particle

Uniform irradiation of such a sample is the simplest type of irradiation exposure to perform. Such exposures have been used for many years. When only beams with short ranges are available, the samples may be thin films of dried amino acids, enzymes or viruses, monolayers of microorganisms, or cultured mammalian cells. For details of the techniques of exposure and dosimetry at the heavy-ion linear accelerators see Birge and Sayeg (1959), Brustad (1961), and Todd et al. (1968). Accelerators with more penetrating radiation allow the uniform irradiation of thin vessels containing powders or aqueous solutions, frozen solutions, suspensions of cells, and thicker masses of cells. Uniform irradiation of small animals can be done by using energetic charged-particle beams (Taketa et al., 1967;Ashikawa et al., 1967; Williams et al., 1966; Mitchell et al., 1966).

Accelerator beams often are of small cross section and are not of uniform intensity over the desired target area. The uniformity of the dose over the sample is achieved either by using a scattering foil upstream at a distance from the sample or by defocusing the beam or by magnetically scanning the beam (Larsson, 1961; Brustad, 1961; Williams et al., 1966).

The dose received by the sample is usually determined by using a thin parallel-plate ionization chamber just in front of the sample. The saturation problems of ionization chambers limit their usefulness at high instantaneous dose rates encountered in pulsed accelerator beams (Boag, 1966). Secondary emission monitors (SEM) are useful at such a high dose rate. The SEM is calibrated by using an ionization chamber at a low dose rate where the saturation is negligible. A Faraday cup is also useful for monitoring the dose; it can be placed behind the sample, or the sample holder can be made to serve as a Faraday cup (Brustad, 1961). The dose is calculated from the measured number of particles and by knowing the average dE/dx pf the particles, from equations (3)-(6).

For very high energy charged-particle beams (e.g., 730-MeV protons),where significant nuclear secondaries are produced, there is a region of dose buildup (Tanner et al., 1967). This buildup varies significantly according to the geometry of the biological sample. Hence phantoms used in dosimetry should have a geometry similar to the biological test object (Ashikawa et al., 1964).

5.2. Samples Much Larger Than the Range of the Particle

Uniform irradiation of liquid sample can be achieved by using a small magnet stirrer during exposure. Such a technique was used in inactivation of enzymes in dilute aqueous solutions (Brustad,

1967).

Powders and thick layers of packed cells cannot be irradiated uniformly. However, in some experiments such as destruction of free radicals or inactivation experiments in microorganisms, it may still be possible to analyze the results when one can estimate the unexposed fraction of the sample (Horan, 1969, private communication).

Another type of irradiation under this category is used when, although the sample may be thick, the target of interest is on or near the surface (Slater et al., 1964; Hirono et al., 1970). Solar flare exposures can result in high dose to the skin. This type of exposure can be simulated with heavy charged particles, since the depth of penetration can be controlled (d'Angio et al., 1964).

Whole skin exposures are normally done by using large radiation fields and rotating the animal about its major axis. The irregular contours of the animal prevent the achievement of uniform surface dose. Because of rotation and irregular contours, the depth-dose pattern deviates considerably from the typical Bragg curve. Depth-dose measurements for such exposures are made with dosimetric systems such as glass rods, lithium fluoride, or other solid-state integrating dosimeters in phantoms. The usefulness of these dosimeters is limited because of their dependence for sensitivity upon the LET of radiation. In order to apply the necessary correction, the LET spectrum to which the dosimeter is exposed and the LET response of the dosimeter should be known. Because of these difficulties in dosimetry, the dose distribution can often be determined by calculation when the physical properties of the beam and the geometric factors of exposure are known (Mitchell et al., 1966).

5.3. intermediate Cases

When the range of the particles is similar to the thickness of the sample, the dose will vary with depth. However, techniques are available whereby one can transform such a distribution and obtain various other types of dose distributions by summing the depth-dose distributions of beams of different energies.

The procedure of obtaining a uniform depth-dose distribution over a given volume is to superimpose a series of Bragg peaks with progressively smaller intensities and shorter ranges (see Fig. 3.6). With such uniform depth-dose distribution, uniform whole-body irradiation of animals is possible as long as the primary energy of the beam is sufficient to penetrate the animal. However, it must be noted that the LET of the radiation increases with depth. This

variation is reduced by rotating the animal during exposure.

The dose due to solar flare events monotonically decreases with depth. Such a depth-dose distribution can also be obtained in the laboratory by superimposition of Bragg peaks. Short range Bragg peaks of great intensity are used (see Fig. 3.7). Such a depth-dose distribution obtained by using helium ion beams has been used to simulate solar flare exposures in monkeys (Aceto et al., 1971).

One method of obtaining the desired dose distribution is to sequentially degrade the full-energy beam by a series of absorbers (uniformly incremented) (Jansen, 1960). Another method has been the use of a variable-thickness water absorber in place of the solid absorbers. Such an absorber can be constructed in the form of a cylinder and a piston. Both the end of the cylinder and the end of the piston are made of reasonably thin material. The cylinder is filled with water and is maintained full by a reservoir located above the cyclinder. The position of the piston determines the amount of water in the beam path. The piston position is programmed to be varied in an appropriate manner as a function of the cumulative particle flux incident on the absorber (Larson,1961).

The most useful method for producing desired depth-dose distributions employs a ridge filter (Karlsson, 1964). This filter consists of a series of similar units, usually made of a dense metal such as copper or the tungsten alloy known as "heavy metal." These units are placed side by side to form a composite filter whose cross section is larger than the beam area. Each unit is essentially a stepwise variable-thickness absorber. The width of an individual step determines the relative intensity, and the total thickness of the step determines the residual energy and therefore the residual range of that portion of the beam that passes through that step. The use of a ridge filter permits the simultaneous superposition of the depth-dose distributions of all the components required to produce the desired depth-dose distribution. As more components are used to approximate the desired distribution, the number of steps increases and the cross section of the individual units more closely approximates a smooth curve rather than a stepped pyramid.

In solar flare simulation experiments with monkeys, the helium-ion Bragg curve was transformed into an exponentially decreasing depth-dose distribution. The monkey was rotated on its major axis to simulate an omnilateral exposure. Isodose contours for such an exposure are shown in Fig. 3.8. It should be noted that unshielded parts of the body with small contours, such as the tail and neck, receive higher doses to both the midline and the surface. Arms and legs are generally shielded by the body and hence receive

doses similar to the rest of the body.

6. Future Accelerators

No existing accelerator can produce beams of heavy ions above atomic number 18 with sufficient energy to penetrate biological tissue deeply enough to allow significant assessment of the biological effects. Yet it was shown in Chapter 2 that significant numbers of high-energy heavy nuclei exist in primary cosmic rays up to $Z = 26$ (iron), and that radiation from even heavier nuclei, up to perhaps transuranium atomic numbers, is a problem for long-term space flights, particularly with respect to injury to the nervous system. One could raise the question: Is it necessary to accelerate the heaviest nuclei in order to study their biological effects, or can one simulate their effects, quantitatively, by some other method?

6.1. Limitations of Existing Methods

Zeman et al. (1961) have attempted to simulate the effect of very heavy ionizing tracks by working with beams of deuterons of about 20 MeV energy, using these to expose rat cerebral cortex. Although the biological results obtained in this work appear interesting, one may show on physical grounds that in practice such collimated beams could not produce, quantitatively, the same ionization effects as the heavy particles themselves. Assume that we wish to simulate the effect of an iron particle at 10 MeV/nucleon ($Z = 26$). The ionization of such a particle corresponds to that from $n = Z^2$ deuterons--that is, $n = 676$ deuterons--of the same energy per nucleon, 10 MeV/nucleon. However, for a realistic simulation of the effects it would be necessary to have all these particles arrive in as small a region of space as the region where a single iron nucleus exerts its primary ionization and to do this within as short a time as it takes for the primary ionization effects to occur from an iron particle. The irradiation must be over before relatively stable radiochemical products appear.

The primary ionization at the core of the track occurs very close to the track in solids and liquids, probably within a few angstroms, since at greater distances the atomic electron clouds in the absorber exert a considerable screening effect. As the limiting screening distance is somewhat uncertain, assume 10 A for this calculation, or a cross-sectional area of $\sigma = 10^{-14}$ cm^2 for the "core of primary ionization events." There is also much evidence to indicate that, radiochemically as well as biologically, in aqueous systems at room temperature, the essential radiation lesion is complete within $t = 10^{-7}$ sec. The particle flux density in the

simulating deuteron microbeam would then need to be

$$F = n(\sigma t) = +676/(10^{-14} \times 10^{-7}) = 6.8 \times 10^{23} \qquad (3-7)$$

particles/ cm^2-sec. The pulsed beam of 1 mm^2 cross section would thus need intensities of about 1000 A of accelerated particles. This is several orders of magnitude higher than provided by conventional cyclotrons. It is a possible design goal for the future, but the equipment would appear to be more expensive than the cost of providing an accelerated beam of even the heaviest ions. If the simulation is attempted at lower beam intensities, then, locally, at the time scale of the atoms and molecules of the organism, a good part of the effect of each deuteron might be accomplished and over before the next deuteron appeared. A further complication in actual use of microbeams is that it seems impossible to hold the particles of a microbeam of cross-sectional dimensions of less than 1 micron together for penetration distances of 0.1 cm or more, because the multiple scattering tends to broaden the beam to several microns. Thus, we must conclude that in order to study heavy-ion effects, one needs to use the actual fast heavy ions, either in cosmic rays or from accelerators.

A second question arises whether or not it is necessary to reproduce in the laboratory the heavy ions at the same energies as they occur at in space (probably several hundred to several thousand MeV/nucleon). Although it would be interesting to have such ions in the laboratory, the biophysicist needs at present more modest energies: the unknown domain of biological effects is in the relatively low-energy region of heavy particles, where the rate of energy loss to tissue is greatest. One must, of course, have particles of sufficient penetration so that the particles can reach to organs and biological structures, where knowledge of the effects appears essential. For example, exposure of significant portions of the mammalian brain and spinal cord and reproductive system appear necessary. In order to achieve this, particle energies up to several hundred MeV/nucleon are required.

6.2. The Acceleration of Heavy Ions

Acceleration of heavy ions presents some special problems different from those encountered in the acceleration of electrons, protons, or helium ions. Because the acceleration is usually based on electrical forces, the efficiency of acceleration depends upon the degree of stripping (electron removal). Conventional low-voltage ion sources can produce adequate numbers of doubly stripped ions. The remaining electrons surrounding heavy nuclei can be removed in high-velocity collisions between the ions and the electrons in a

"stripping foil" through which the ions can be made to pass. An ion is not likely to lose all its electrons in a collision unless the velocity of the ion is greater than that of its atomic K-shell electrons.

One of the first schemes for accelerating heavy ions by the use of stripping was suggested in 1951 (Tobias, 1951). With this scheme one cyclotron could be used to accelerate heavy ions with a low charge-to-mass ratio and then inject this beam into another cyclotron where the ions could be stripped and accelerated to high energies in a more efficient fashion. During recent years it was clearly demonstrated that accelerators for heavy ions can be constructed in many configurations (Livingston, 1969).

In one proposed accelerator ("Omnitron") a synchrotron ring is combined with a storage ring. Acceleration is carried out in two steps: first, ions with a low charge-to-mass ratio are accelerated by the synchrotron principle to an energy of several MeV/nucleon, then they are shunted to a storage ring while the magnetic field of the synchrotron is reset; the ions from the storage ring are then stripped, reinjected into the synchrotron ring, and accelerated again. With this method it is feasible to obtain particles of 500 MeV/nucleon with significant beam intensities, and all atoms in the periodic table can be accelerated (see Omnitron, 1966).

Recently it has been shown that the existing heavy-ion linear accelerator at Berkeley can be modified by redesigning the linear tanks and inserting an additional stripping station so that it can accelerate all atoms in the periodic table to a kinetic energy of about 8.5 MeV/nucleon with intensities of the order of 10 to 100 μA of beam current. Studies indicated that it is feasible to inject the ions from this linear accelerator to a synchrotron ring and to accelerate up to 500 MeV/nucleon with a ring diameter of about 85 feet. Because the injection energy from the Hilac is not sufficiently high, the heaviest atoms, for example uranium, will not be completely stripped and their kinetic energy will be less than that of lighter atoms. Even so, it is expected that uranium ions of about 140 MeV/nucleon can be accelerated in the heavy-ion synchrotron. The synchrotron would use only a small portion of the Hilac beam for injection, so the final high-energy beam intensity would be only about 1/10 000 of the beam intensity in the Hilac. However, this is still ample intensity to conduct most biological studies. The proposal to build such a heavy-ion synchrotron is under consideration, and a schematic diagram of this accelerator is shown in Fig. 3.9.

6.3. New Concepts in Ion Acceleration

Two additional recent methods now under investigation promise

acceleration of very heavy ions to energies greater than 200 MeV/nucleon in a relatively economical manner. One of these, being studied at Stanford, would employ superconducting technology. After an initial preacceleration, which would be accomplished in a conventional manner, a large energy gain of perhaps 6 MeV/nucleon per linear foot of acceleration might be achieved. This scheme depends a great deal on the technology of building supercooled microwave cavities. This technology may provide high-intensity beams of energetic heavy ions.

A potentially far-reaching and relatively new accelerator concept is that of the electron ring accelerator, which has grown from a proposal by Veksler (1956). The basic principle of this machine is the provision of an electron plasma -- a cloud of electrons -- confined by magnetic fields to a small space and the injection of a group of neutral atoms into the electron cloud. The atoms repidly become ionized owing to collisions and become embedded in the electron cloud. The electron plasma is then moved forward and expanded, causing linear acceleration of the ions that are being dragged with it. The concept of the electron ring accelerator (ERA) is being tested experimentally in the USSR and in the USA. In early 1969, USSR scientists reportedly produced a nitrogen ion beam of about 4 MeV/nucleon. The ERA may turn out to be a very efficient generator of accelerated heavy nuclei. There seems to be no limitation on the atomic number of the accelerated ion, except that more electrons are used per ion to accelerate the heavier ions than the light ions. As the acceleration is magnetic, very rapid gains in particle energy seem feasible. For example, in order to obtain an energy of 500 MeV/nucleon it might take only a short linear accelerator of 25 to 50 feet. If the method is proven practical, there seems to be no reason why one should not obtain protons and heavy ions in an energy range of several hundred GeV.

REFERENCES

Aceto, H., G. New, L. W. McDonald, J. T. Lyman, A. Graybiel and C. A. Tobias. Effects of Simulated Solar Flare Radiation on the Squirrel Monkey (*Saimiri sciureus*), in preparation, 1971.

Ashikawa, J. K., C. A. Sondhaus, C. A. Tobias, A. G. Greenfield and V. Paschkes. Difference in Injury Mode, Dose-Rate Dependence and RBE OF **730**-MeV Protons, 100-kVp X-Rays and 250-kVp X-Rays. In *Biological Effects of Neutron and Proton Irradiations*, Vol. 1, p. 240, International Atomic Energy Agency, Vienna, 1964.

Ashikawa, J. K., C. A. Sondhaus, C. A. Tobias, L. L. Kayfetz, S. O. Stephens and M. Donavan. Acute Effects of High Energy Protons and Alpha Particles in Mice. *Radiation Res. Suppl.*, 7:312-324 (1967).

Attix, E. H., W. C. Roesch and E. Tochilin. *Radiaton Dosimetry*, Vol. 2, Academic Press, New York (1966).

Barkas, W. H. and M. J. Berger. Tables of Energy Losses and Ranges of Heavy Charged Particles. Studies in Penetration of Charged Particles in Matter, National Academy Science-National Research Council, Publ. 1133, p. 103 (1964).

Benson, R. E., R. G. Thomas and L. T. Odland. Proton-Induced Radioactivity in Primates. *Health Phys.*, 13:1123-1125 (1967).

Bewley, D. K., S. B. Field and C. J. Parnell. Physical Aspects of the Deuteron and Helium Nuclei Beams from the M. R. C. Cyclotron. *Phys. Med Biol.*, 12:1 (1967).

Bichsel, H. Charged Particle Interactions, in *Radiation Dosimetry*, Vol. 1, E. H. Attix and W. C. Roesch (Eds.), Academic Press, New York (1968).

Birge, A. C. and A. Sayeg. The Effects of Accelerated Carbon Nuclei and Other Radiations on the Survival of Haploid Yeast. I. Dosimetry of the Cyclotron Beams. *Radiation Res.*, 10:433–448 (1959).

Boag, J. W. Ionization Chambers, in *Radiaton Dosimetry*, Vol. II, E. H. Attix and W. C. Roesch (Eds.), p. 1, Academic Press, New York (1966).

Bragg, W. H. and R. D. Kleeman. *Phil. Mag.*, 8:726–738 (1904).

Brustad, T. Molecular and Cellular Effects of Fast Charged Particles. *Radiation Res.*, 15:139 (1961).

Brustad, T. Effects of Accelerated Heavy Ions on Enzymes in the Dry State and in Aqueous Solutions. In *Proceedings of the 1st International Symposium on the Biological Interpretation of Dose from Accelerator-Produced Radiation, Berkeley, California*, 1967, p. 30–44

Chamberlain, O., E. Segre and C. Wiegand. Experiments on Proton–Proton Scattering from 120 to 345 MeV. *Phys. Rev.*, 83:923 (1951).

D'Angio, G. J., J. H. Lawrence, A. Gottschalk and J. Lyman. Relative Efficiency of High–LET Radiation (Bragg Peak Lithium Ions) on Normal Rabbit Skin, Using Integral Dose as a Basis for Comparison. *Nature*, 204:1267–1268 (1964).

Gordon, H. S. and G. A. Behman. Particle Accelerators, in *American Institute of Physics Handbook*, 2nd Ed., D. E. Gray et al. (Eds.), McGraw–Hill, New York (1963), pp. 8–168.

Goulding, F S. Semiconductor Detectors for Nuclear Spectrometry. Lawrence Radiation Laboratory Report UCRL–16231, 1965.

Hirono, Y., H. H. Smith, J. T. Lyman and K. H. Thompson. The Relative Biological Effectiveness of Heavy Ions in Producing Mutations, Tumors and Growth Inhibition in Arabidopsis. *Radiation Res.*,44:204–223 (1970).

Hornstra, F., Jr., J. R. Simanton. Simple, Nondestructive Profile Monitor for External Proton Beams. *Nucl. Instr. Methods*, 68:138–40 (1969).

Jackson, H. G., D. A. Mack and C. Wiegand. Beam Profile Indicator. *Inst. Radio Engrs. Trans. Nucl. Sci.*, 6:64 (1959).

Janni, J. F. Calculations of Energy Loss, Range, Path Length, Straggling, Multiple Scattering and the Probability of Inelastic Nuclear Collisions for 0.1 to 1000 MeV Protons, Air Force Weapons Laboratory Report AFWL–TR 65–150 (1966).

Jansen, C. R., C. Baker, W. Calvo, K. R. Rai and S. Lippincott. Widening Bragg Peak in Path of Charged Heavy Particles in Tissue, Brookhaven National Laboratory Report BNL–5538, 1960.

Jesseph, J. E., W. H. Moore, R. F. Straub, G. M. Tisljar–Lentulis and V. P. Bond. The RBE of 2.2–BeV Protons for 30–Day Lethality in Mice. *Radiation Res.*, 36:242–253 (1968).

Karlsson, B. G. Methoden zur Berechnung und Erzielung einiger fuer die Tiefentherapie mit Hochenergetischen Protonen guenstiger Dosisverteilungen. *Strahlentherapie*, 124:481 (1964).

Koehler, A. M. Dosimetry of Proton Beams Using Small Silicon Diodes. *Radiation Res. Suppl.*, 7:53 (1967).

Larsson, B. Pretherapeutic Physical Experiments with High Energy Protons. *Brit. J. Radio.*, 34:143–151 (1961).

Litton, G. M., J. Lyman and C. A. Tobias. Penetration of High Energy Heavy Ions with the Inclusion of Coulomb Nuclear and Other Stochastic Processes. Lawrence Radiation Laboratory Report UCRL–17392 Rev, 1968.

Livingston, R. S. A Survey of Methods of Accelerating Heavy Ions. International Cyclotron Conference, Oxford, England, Sept. 17–19, 1969, Oak Ridge National Laboratory Report ORNL–TM–2686, 1969.

Lyman, J. T. Dark Recovery of Yeast Following Ionizing Radiations (Ph.D. Thesis). Lawrence Radiation Laboratory. Report UCRL-16030, 1965.

Maccabee, H. D., M. R. Raju and C. A. Tobias. Fluctuations of Energy Loss by Heavy Charged Particles in Thin Absorbers. *Phys. Rev.*, 165:469-74 (1968).

Mitchell, J. C., G. V. Dalrymple, G. H. Williams, J. D. Hall and I. L. Morgan. Proton Depth-Dose Dosimetry. *Radiation Res.* 28:390-405 (1966).

Northcliffe, L. C. Passage of Heavy Ions Through Matter. *Ann. Rev. Nucl. Sci.*, 13:67 (1963).

The Omnitron. Lawrence Radiation Laboratory Report UCRL-16828, July 1966.

Palmieri, J. N. and R. Goloskie. Calibration of 30-cm Faraday Cup. Rev. Sci. Instr., 35:1023 (1964).

Preston, W. M., and A. M. Koehler. The Effects of Scattering on Small Proton Beams, Harvard University Cyclotron Laboratory Report, 1968.

Raju, M. R. Heavy-Particle Studies with Silicon Detectors. *Radiation Res. Suppl.*, 7:43 (1967).

Raju, M. R. The Use of the Miniature Silicon Diode as a Radiation Dose Meter. *Phys. Med. Biol.*, 11:371 (1966).

Raju, M. R., J. T. Lyman, T. Brustad and C. A. Tobias. Heavy-Charged-Particle Beams. In *Radiation Dosimetry*, Vol. 3 (E. H. Attix, W. C. Roesch and E. Tochilin, Eds.). Academic Press, N.Y. (1969).

Rossi, B. *High-Energy Particles*. Prentice-Hall, Englewood Cliffs, N. J. (1952).

Santoro, R. T. The Space, Time and Energy Distribution of the Beam of the Harvard University Synchrocyclotron. Oak Ridge National Laboratory Report ORNL-3722, 1965.

Santoro, R. T., F. E. Bertrand, T. A. Love and R. W. Peele. Beam Energy Measurements at the Oak Ridge Isochronous Cyclotron. Oak Ridge National Laboratory Report ORNL-TM-1382, 1966.

Santoro, R. T. and R. W. Peele. Measurement of the Intensity of the Proton Beam of the Harvard University Synchrocyclotron for Energy-Spectral Measurements of Nuclear Secondaries. Oak Ridge National Laboratory Report ORNL-3505, 1964.

Slater, V., J. Lyman, C. A. Tobias, N. M. Amer, J. S. Beck, M. Beck, and A. J. Slater. Heavy-Ion Localization of Sensitive Embryonic Sites in *Tribolium*. *Radiation Res.*, 21:541-549 (1964).

Steward, P. Stopping Power and Range for Any Nucleus in the Specific Energy Interval 0.01-500 MeV/amu in Any Nongaseous Material (Ph.D. Thesis). Lawrence Radiation Laboratory Report UCRL-18127, 1968.

Taketa, S. T., L. Castle, H. Howard, C. C. Conley, W. Haymaker and C. A. Sondhaus. Effects of Acute Exposure to High Energy Protons on Primates. *Radiation Res. Suppl.*, 7:336-359 (1967).

Tanner, R. L., N. A. Bailey and J. W. Hilbert. High-Energy Proton Depth-Dose Patterns. *Radiation Res.*, 32:861-74 (1967).

Tautfest, G. W. and H. R. Fechter. A Nonsaturable High-Energy Beam Monitor. *Rev. Sci. Instr.*, 26:229 (1955).

Tilbury, R. S. Activation Analysis with Charged Particles. U. S. Atomic Energy Commission Report NAS-NS 3110, 1966.

Tobias, C. A. Acceleration of Multiply Charged Nuclei. *Bull. Am. Phys. Soc.*, 26 8:16 (1951).

Tobias, C. A., H. O. Anger and J. H. Lawrence. Radiobiological Use of High Energy Deuterons and Alpha Particles. *Am J. Roentgenol. Radium Therapy and Nucl. Med.*, 68: 1–27 (1952).

Tobias, C. A., P. Rosahn, M. Lewis, H. O. Anger and J. H. Lawrence. Biological Use of High Energy Deuterons, University of California Radiation Laboratory Report UCRL–193, 1948.

Todd, P. W., T. Lyman, A. Armer, D. Skarsgard and R. A. Deering. Dosimetry and Apparatus for Heavy Ion Irradiation of Mammalian Cells *in vitro*. *Radiation Res.*, 34:1–23 (1968).

Trower, W. P. High–Energy Particle Data, Vols. I–IV. Lawrence Radiation Laboratory Report UCRL–2426 Rev., 1966.

Veksler, V. I. In *Proceeding of the CERN Symposium on High Energy Accelerator and Pion Physics, Geneva.* CERN Scientific Service, Geneva (1956). Vol. 1, p. 80.

Williams, G. H., J. D. Hall and I. L. Morgan. Whole–Body Irradiation of Primates with Protons of Energies to 400 MeV. *Radiation Res.*, 28:372–389 (1966).

Williamson, C. F., J. P. Boujot and J. Picard. Tables of Range and Stopping Power of Chemical Elements for Charged Particles of Energy 0.5 to 500 MeV. Rapport CEA–R3042, Centre d'Etudes Nucleaires de Saclay, 1966.

Wilson, R. R. Radiological Use of Fast Protons. *Radiology*, 47:487 (1946).

Zeman, W., H. J. Curtis and C. P. Baker. Histopathologic Effect of High–Energy–Particle Microbeams on the Visual Cortex of the Mouse Brain. *Radiation Res.*, 15:496–514 (1961).

Table 3.1. Some Western Accelerators Used for Biological Research.

Location and name	*Particles and energy*	*Biological applications*
Berkeley LRL 184-inch cyclotron	730-MeV protons 450-MeV deuterons 910-MeV helium ions Π mesons	simulated solar flares, mammalian and cellular radiobiology, brain studies, therapy
Berkeley LRL 88-inch cyclotron	55-MeV protons 60-MeV deuterons 120-MeV helium ions 180-MeV Li ions	skin lesions, local brain irradiation
Berkeley-LRL Yale University	10.4-MeV/nucleon Max Ions of D, He, Li, B, C, N, O, Ne, S, Ar	macromolecules, microorganisms, mammalian cells, seed mutagenesis, insect development
Brookhaven 60-inch cyclotron	24-MeV deuterons 48-MeV helium ions	laminar brain lesions, skin studies
Newport News, Va. NASA cyclotron (VARC)	300-MeV, 600-MeV protons	special mammalian studies, cataract formation
College, Texas Southwest 90-inch cyclotron	120-MeV max helium ions	planned
Chicago Univ. Chicago cyclotron	400-MeV protons	shielding studies

Table 3.1 Cont'd.

Location and name	*Particles and energy*	*Biological applications*
Cambridge, Mass. Harvard Univ. cyclotron	160-MeV protons	enzymes, brain studies, therapy
Uppsala, Sweden Gustav Werner cyclotron	189-MeV protons	brain studies endocrinology, therapy
Orsay, France cyclotron	150-MeV protons	animal radiobiology
Geneva, Switzerland CERN cyclotron	600-MeV protons	meson radiobiology, mutagenesis
London Hammersmith Hosp. cyclotron	18-MeV deuterons	neutron studies skin, tumor, and cellular radiobiology, neutron therapy
Harwell, England AERE cyclotron	150-MeV protons	chromosome studies, cellular radiobiology

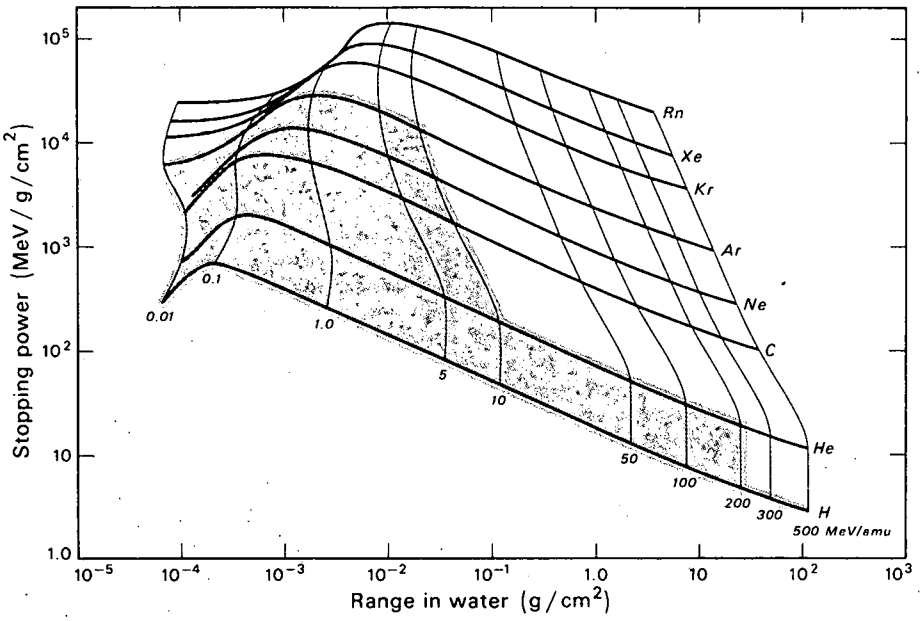

Fig. 3.1. Theoretical range energy and stopping power for various heavy ions in water (Steward, 1967). Shaded area indicates the energies of the currently available heavy-charged-particle beams.
(DBL682-4598)

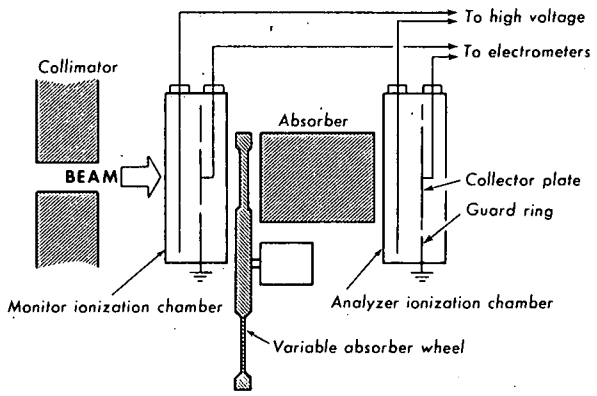

Fig. 3.2. Experimental arrangement for measuring the Bragg curve.
(MUB-13671)

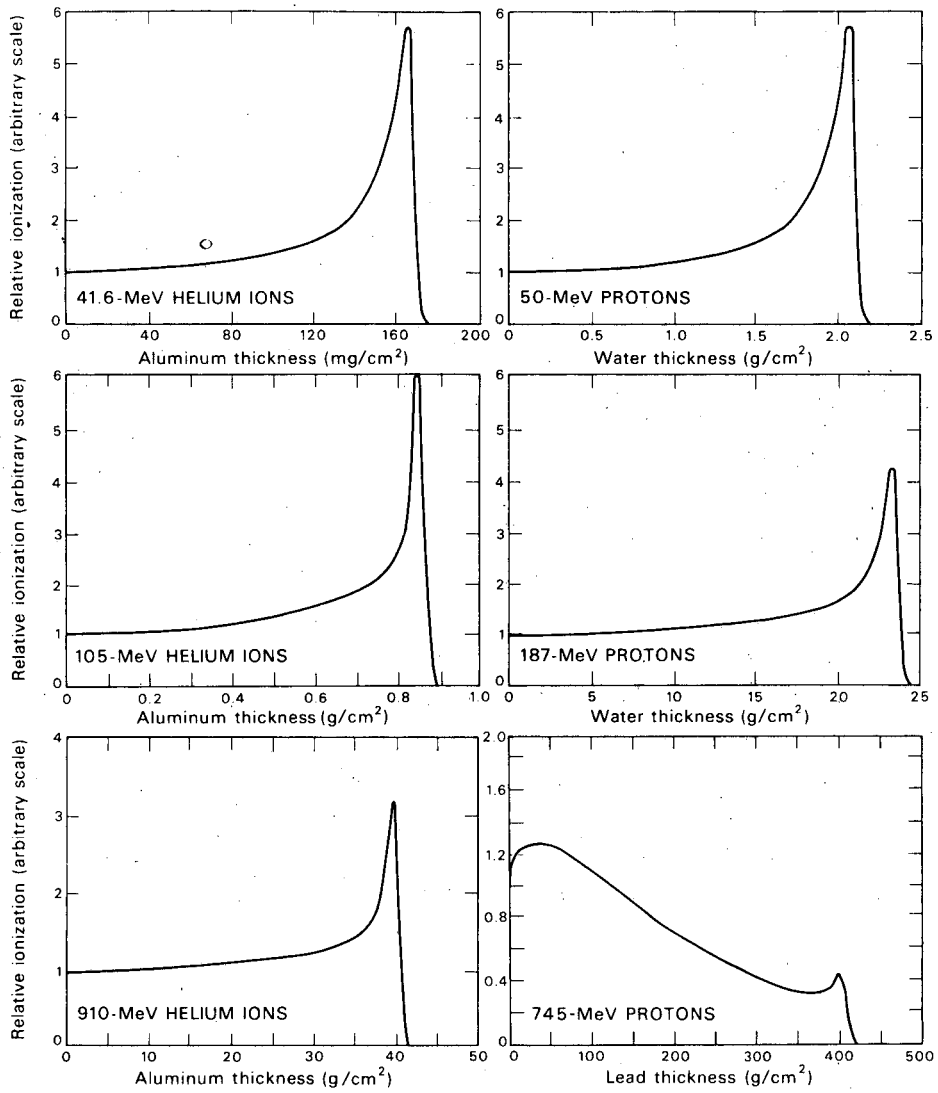

Fig. 3.3. Depth-dose distribution of proton and helium ion beams. The depth-dose distribution of a high-energy proton beam (730 MeV) in copper is very different in shape from the other curves. The initial dose buildup is due to secondary-particle production, and the reduction of dose with depth is due to loss of particles through nuclear interactions as described in the text.

(DBL6711-1885)

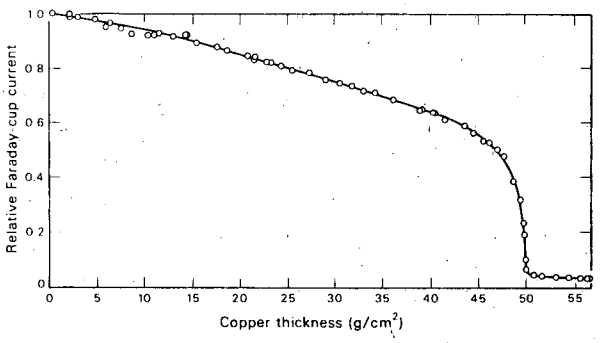

Fig. 3.4. Charge collected in a Faraday cup versus copper absorber thickness for a 910-MeV helium-ion beam. This is very similar to the number-distance curve, since the charge of these energetic ions remains essentially the same until the last few mg/cm^2 of the total range. Notice the slope to the left of the knee ($\approx$ 42 g/cm^2) resulting from nuclear interactions.

(DBL6711-1888)

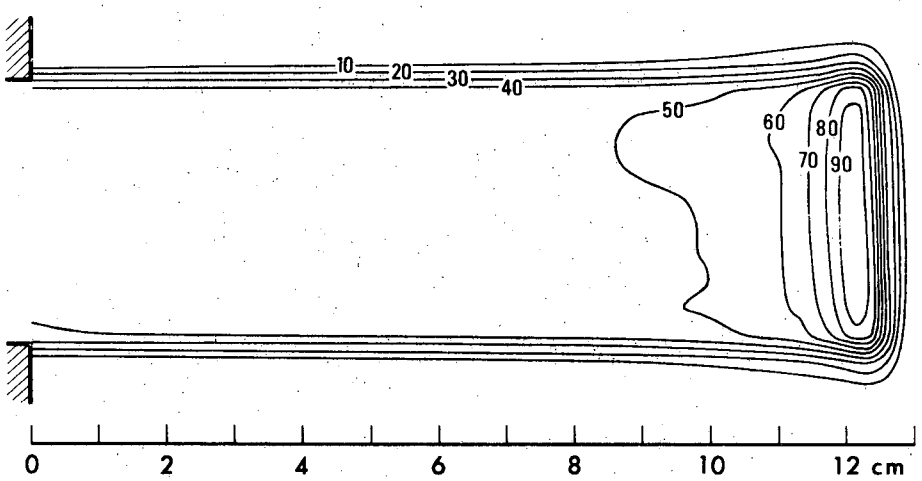

Fig. 3.5. Isodose contours in water of a 910-MeV helium-ion beam degraded to $\approx$ 400 MeV by 32 mm of copper.

(DBL678-1717)

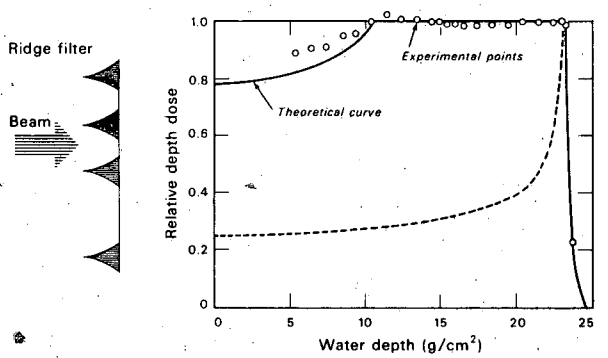

Fig. 3.6. Depth-dose distribution of 187-MeV proton beam in water, together with modified depth-dose distribution obtained by using ridge filter made of Hevimet (90% W, 7% Ni, and 3% Cu), redrawn from Karlsson (1964). The maximum thickness of the ridge filter is 13 mm, the base of each unit is 6 mm wide, and the units are separated by 2 mm.

(DBL6711-1892)

Fig. 3.5. Isodose contours in water of a 910-MeV helium-ion beam degraded to ≈ 390 MeV by 32 cm of copper.
(DOE 678-1417)

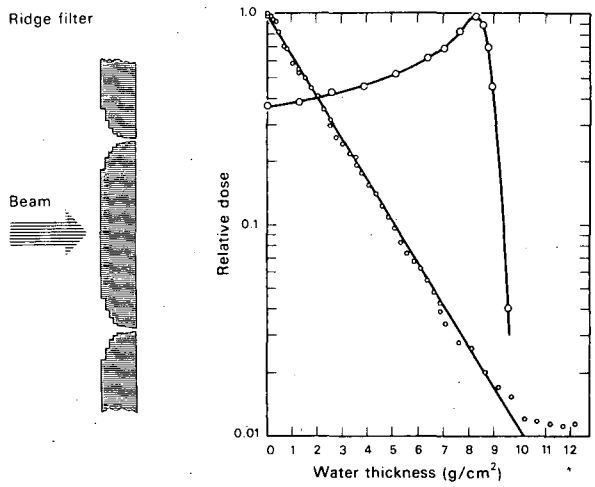

Fig. 3.7. Depth-dose distribution of degraded (38.1 mm of copper) 910-MeV helium-ion beam (large circles) together with modified depth-dose distribution obtained by using a copper ridge filter (small circles). The maximum thickness of the ridge filter is 14.3 mm, the width of an individual unit is 50.8 mm, and the separation between the individual units is 0.1 mm.

(DBL6711-1890)

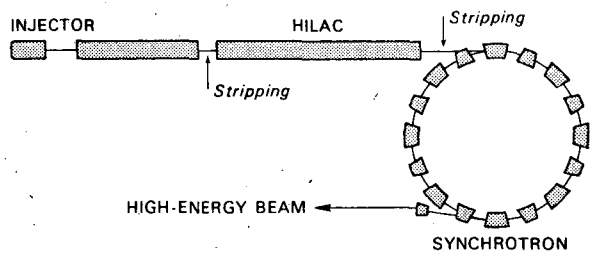

Fig. 3.9. Schematic diagram of heavy-ion synchrotron.

(DBL 704-5697)

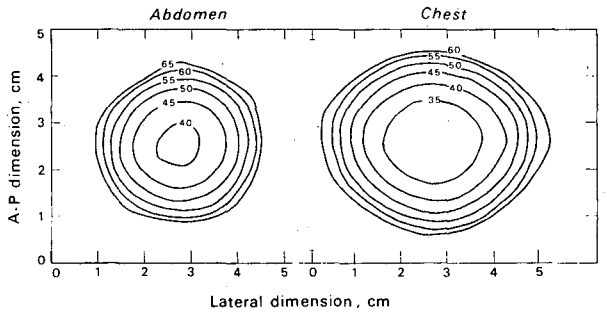

Fig. 3.8. Isodose contours. X and Y axes are in centimeters.

(DBL701-5537)

TECHNICAL INFORMATION DIVISION
LAWRENCE BERKELEY LABORATORY
UNIVERSITY OF CALIFORNIA
BERKELEY, CALIFORNIA 94720